Effect of Internal Reflections on the Radiation Properties and Input Impedance of Integrated Lens Antennas—Comparison Between Theory and Measurements

Maarten J. M. van der Vorst, *Member, IEEE*, Peter J. I. de Maagt, *Member, IEEE*, Andrea Neto, *Member, IEEE*, Andrew L. Reynolds, Rob M. Heeres, Willem Luinge, and Matti H. A. J. Herben, *Senior Member, IEEE*

***Abstract*—This paper presents the effect of internal reflections on the beam pattern and input impedance of integrated lens antennas. A silicon lens was designed and manufactured, and measurements were conducted at a frequency of 100 (impedance) and 500 GHz (beam pattern). A frequency-dependence characterization of the beam pattern clearly showed the existence and impact of internal reflections. The measurements confirmed that most of the frequency variations of the beam pattern could be attributed to internal reflections, as predicted by the model. An on-wafer measurement strategy for determining the antenna impedance at millimeter-wave frequencies is presented. The validity of the model was also proven by an excellent match of the input impedance measurements and predictions. Not only the level, but also the oscillation on the impedance curve was predicted accurately. Initial space qualification was performed in the form of thermal cycling.**

***Index Terms*—Integrated lens antennas, internal reflections and input impedance.**

I. Introduction

MILLIMETER-WAVE and submillimeter-wave frequencies are becoming increasingly important in various applications. For example, in imaging, remote sensing, radio astronomy, and radar there is a high demand for low-noise receivers operating at frequencies from 30 GHz to 3 THz [1]–[4]. There are several very important processes taking place in the atmosphere that deserve our attention, such as the greenhouse effect and ozone depletion. There is an ever-growing awareness on the possible detrimental effects of man's activities on climate. (Sub)millimeter-wave frequencies can be used to obtain data for studies on ozone-depletion mechanisms. Millimeter-wave frequencies can focus on exchanges between troposphere and stratosphere, bringing complementary information useful for studies on global changes.

One of the most challenging problems in cosmology is the issue of small temperature anisotropies in the cosmic microwave background. The combination of millimeter and submillimeter-wave frequencies allow contamination from galactic emission and extragalactic sources to be removed from the cosmological temperature anisotropies. Space astronomy observations at submillimeter wavelengths will also open up a virtually unexplored part of the spectrum, which cannot be observed well from the ground.

Several Earth observation instruments (MASTER, SOPRANO, PIRAMHYD) and astronomical missions (FIRST, PLANCK), which use millimeter and submillimeter wavebands, are being planned by the European Space Agency (ESA), Noordwijk, The Netherlands. These instruments have many commonalities in their design and construction techniques. They require state-of-the-art technology to achieve their ambitious goals; the highest resolution, sensitivity and frequency of operation.

Most of the above-mentioned instruments have receivers that work with horn antennas as receiving elements. They have traditionally been the most common microwave antenna feed types and, although the attenuation of fundamental-mode waveguides at higher frequencies is high and both the effect of metal tolerances and misalignments becomes more severe, horns and waveguides have been produced for these wavelengths [5]. In view of the cited difficulties, there is a need for alternative technologies and planar integrated technology is expected to offer a good solution.

In recent years, the advancement of photolithographic and micromachining techniques has resulted in very reliable and repeatable processes for creating planar structures on dielectric substrates. The fabrication of very complex electronic structures with a high yield is now possible. Within the field of submillimeter-waves (30 GHz–3 THz), antenna and other high-frequency component manufacturing has been limited both by the complexity of fabricating small accurate structures and the expense thereof. However, the progress in planar technology now

Manuscript received January 17, 2000; revised September 21, 2000. This work was supported in part by the European Space Agency under Contract 11653/95/NL/PB.

M. J. M. van der Vorst was with the Eindhoven University of Technology, 5600 MB Eindhoven, The Netherlands. He now is with the European Space Research and Technology Centre, European Space Agency, 2200 AG Noordwijk, The Netherlands.

P. J. I. de Maagt and A. Neto are with the European Space Research and Technology Centre, European Space Agency, 2200 AG Noordwijk, The Netherlands.

A. L. Reynolds is with the Faculty of Electrical Engineering, University of Glasgow, Glasgow G12 8LT, Scotland.

R. M. Heeres is with the Department of RF Modules, Philips Discrete Semiconductors, 6534 AE Nijmegen, The Netherlands.

W. Luinge is with the Space Research Organization of the Netherlands, 9700 AV Groningen, The Netherlands.

M. H. A. J. Herben is with the Faculty of Electrical Engineering, Radiocommunications Group, Eindhoven University of Technology, 5600 MB Eindhoven, The Netherlands.

Publisher Item Identifier S 0018-9480(01)03994-1.

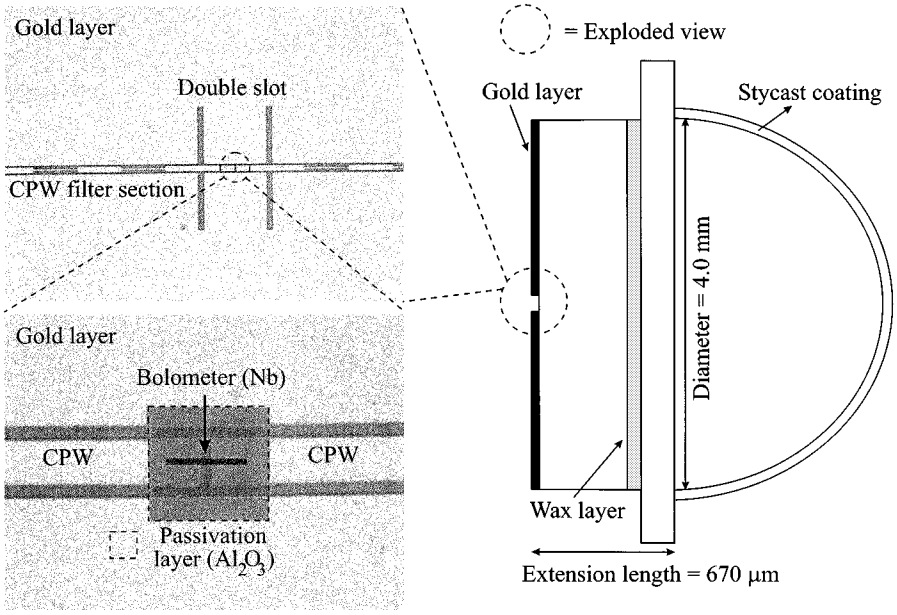

Fig. 1. Integrated lens antenna design with expanded view of double slot and bolometer detector (dimensions not to scale).

allows these components to be accurately produced in much larger numbers at far lower costs.

However, there might be some problems related with planar antennas because of the reduced efficiency associated with the dielectric substrates on which these antennas are fabricated. If the dielectric is thick in terms of a wavelength, surface waves can be excited. Two basic approaches have been used to increase the efficiency; dielectric lenses or photonic-bandgap (PBG) crystals. The PBG antenna is still a relatively new concept and, with respect to the antenna performance the PBG technology, is still in an experimental stage. Conversely, research on integrated lens antennas and designs has already reached some level of maturity and very promising radiation characteristics have been demonstrated.

In this paper, the electromagnetic model of the internal reflections in integrated lens antennas, as described in [6], is compared to measurements. First, the planar feed design at 500 GHz is treated. In Sections III and IV, the beam-pattern measurements are discussed, while the input impedance measurement results are compared to theoretical results in Section V. Finally, conclusions are drawn in Section VI.

II. Integrated Lens Antenna Design

A. General

Many scientific applications, such as limb sounding, radiometry, and radio astronomy require an antenna that is optimized for that particular application. Previous work on integrated lens antennas [3], [4] showed that a high dielectric-constant lens like silicon ($\varepsilon_r = 11.7$) is very suitable to achieve excellent performance in the millimeter and submillimeter range. The substrate lens, which is very attractive because of its mechanical rigidity and thermal stability, is designed for a limb-sounding instrument in the following section. The main design objectives for that application were the Gaussian beam efficiency ($\eta_{\rm gauss}$) and the beam efficiency ($\eta_{\rm beam}$). Furthermore, a beam waist (w_0) of 1.20 mm was required to couple well to an existing quasi-optical system ([7]).

B. Planar Feed and Lens Design

The lens antenna was optimized for an operating frequency of 500 GHz. A planar double-slot radiator is selected as a feed for a (high-resistivity) silicon substrate lens. The double-slot antenna was chosen above other configurations, such as a double dipole, an annular slot, etc., because of its better characteristics in terms of the beam and Gaussian beam efficiency. After the optimization procedure, as described in [8], a double-slot length, separation, and width of 168, 93, and 8 μm followed, respectively. This resulted in an expected coupling efficiency of over 90% to the $2 \times 1\mu$m niobium (Nb) bolometer.

The resulting lens geometry from the design procedure consisted of an extended hemispherical silicon lens with a diameter and extension length of 4.0 mm and 670 μm, respectively. On top of the lens, a quarter-wavelength (88 μm) coating of Stycast 1264 is applied. The actual design is depicted in Fig. 1, which includes the exploded view of the double-slot feed and bolometer. The bolometer is placed between the inner conductors of the coplanar waveguides (CPWs) connecting the slot elements.

The transmission and absorption of Stycast 1264 were measured at room temperature with a Michelson interferometer in the frequency range from 300 to 1500 GHz (Fig. 2). From those measurements, a relative dielectric constant of 2.90 was found, while the absorption coefficient was 3.5 Np/cm. The same measurements, but at a temperature of 4 K, showed that the permittivity decreased to 2.85 and the absorption coefficient to 0.2 Np/cm (Fig. 3).

To test whether the silicon/Stycast 1264 combination could withstand thermal cycling from room to cryogenic temperatures, the silicon lens with a layer of Stycast 1264 was heated and cooled down from 300 to 4 K. No delaminating or cracking was observed after multiple cool downs to 4 K.

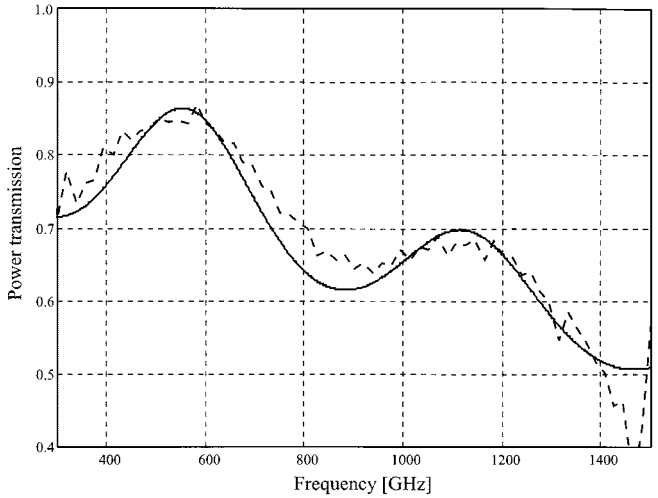

Fig. 2. Power transmission spectrum of Stycast 1264 layer with thickness of 152 μm at 300 K (—: fitted theoretical curve, – –: measured data).

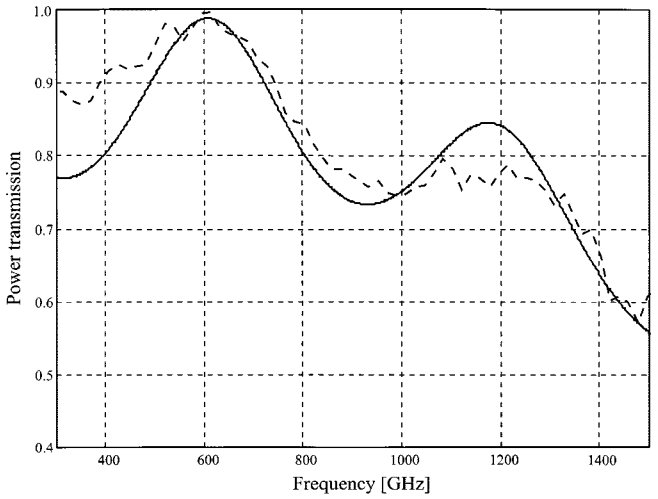

Fig. 3. Power transmission spectrum of Stycast 1264 layer with thickness of 148 μm at 4 K (—: fitted theoretical curve, – –: measured data).

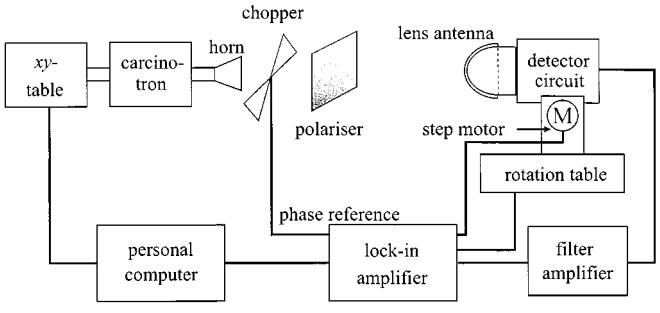

Fig. 4. Beam-pattern measurement setup.

III. Beam-Pattern Measurements

A. Description of the Setup

In the setup, as depicted in Fig. 4, beam patterns are measured with a rotation stage in which the integrated lens antenna can be rotated around two axes. In this way E-, H-, as well as D-plane cross-section measurements can be made. A carcinotron in the frequency range of 400–500 GHz is used as an RF source. The beam coming out of the carcinotron can be collimated ($\pm 10^{\circ}$) and a power density of about 1 $\mathrm{W/m^2}$ can be achieved at the lens position (15 cm from carcinotron). This results in a maximum power at the feed of 1.26×10^{-5} W. Together with the measured noise equivalent power (NEP) of 10^{-9} $\mathrm{W/\sqrt{Hz}}$ and voltage sensitivity of 5 V/W (3-mA bias current) this resulted in a measurement dynamic range of at least 40 dB.

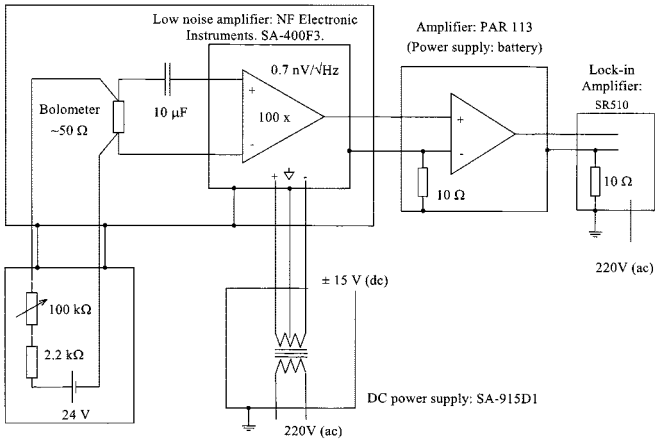

Fig. 5. Detection circuit.

A chopper with a frequency of around 370 Hz is put in front of the horn feed to amplitude modulate the RF signal. This chopper signal is also sent to the phase reference input of the lock-in amplifier. To improve the polarization purity of the feed horn, a polarizer is placed directly after the chopper. The polarized beam is then used to illuminate the integrated lens antenna.

The detection circuit (Fig. 5) was mounted inside a metal housing (metal box), which is covered by an absorbing material to prevent standing waves. The received modulated RF signal is detected by a bolometer and then preamplified. The detector circuit needs a dc-power supply as input and a current source to bias the bolometer. The output signal of the detecting circuit is amplified with a bandpass filter before it is sent to the lock-in amplifier. Furthermore, a computer is used to read/write data from and to the lock-in amplifier.

B. Bolometer Detector

To detect the incoming power at the integrated lens antenna, a microbolometer placed between the two planar slots is used at room temperature. In Fig. 6, the planar feed structure is shown containing the double-slot feed, bolometer detector, and filter section. For the optimum integrated lens antenna design, silicon is selected. Although the conductivity of silicon is somewhat higher than, for example, the conductivity of GaAs, the main contribution of the conductivity losses will come from impurities of the dielectric. Therefore, expensive and pure silicon lenses were used to minimize these losses. To increase the thermal isolation of the bolometer, a 250-nm-thick film of $\mathrm{SiO_2}$ is thermally grown on top of the silicon slab.

The microbolometers used for the actual designs were made of niobium (Nb). One good reason for choosing Nb above the widely used bismuth (Bi) is that, according to [9], the $1/f$ noise level of Nb is a factor of seven lower than the one of Bi. Further, covering the bolometer device with a 10–20-nm-thick layer of

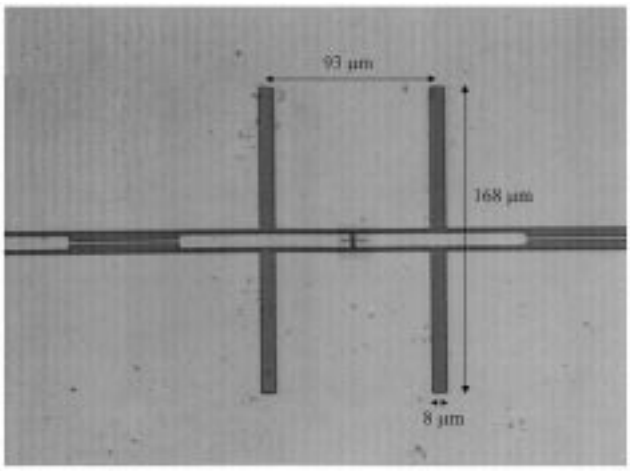

Fig. 6. Double slot plus bolometer detector and filter.

aluminum oxide reduced the oxidation of Nb by air and, consequently, increased the reproducibility and accuracy.

IV. Beam-Pattern Measurement Results

A. Results for Lens without Matching Layer

The first measurements were conducted on a silicon extended hemispherical lens of 4.0-mm diameter. The output frequency of the carcinotron was measured to be 497 GHz and both the co- and cross-polar beam patterns were measured in the E-, H-, and D-planes. In Figs. 7–9, the measured and theoretical results are depicted. It should be noted that the cross-polar radiation in the E- and H-planes was lower than the noise floor of about -40 dB.

Comparing the measurements and predictions in Figs. 7–9 shows that the agreement is very good for both the main beam and sidelobes. Another observation is that, for the measured beams, the nulls are deeper. A possible explanation is the effect of internally reflected field contributions that may interfere with the direct contribution. For a more detailed discussion on the internal reflections, the reader is referred to [6] and Section IV-C. Finally, the differences for larger angles from boresight may be due to a combination of double-slot feed misalignment, the presence of the CPW feeding structure, and the measurement setup.

B. Results for Lens with Matching Layer

The silicon lens coated with the Stycast 1264 material was also measured. The same operating frequency of 497 GHz was used for the measurements and the results for the E-, H-, and D-planes are shown in Figs. 10–12, respectively. The agreement between measurements and predictions for the lens with a matching layer is as good as for the lens without a matching layer.

C. Frequency Dependence

To investigate the frequency dependence of the beam patterns for the lens with and without a matching layer, the measured H-plane co-polar radiation patterns are plotted for the following three frequencies:

1) 475 GHz;
2) 486 GHz;
3) 497 GHz.

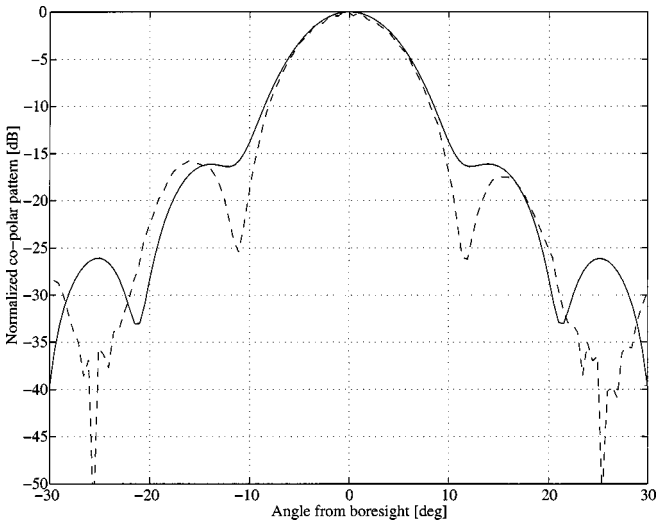

Fig. 7. Computed (—) and measured (– –) E-plane beam patterns at 497 GHz, of a 4.0-mm-diameter silicon hemispherical lens with an extension length of 670 μm.

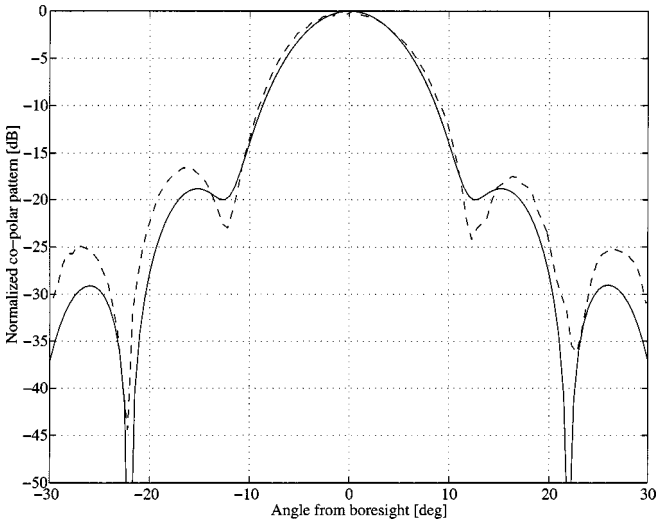

Fig. 8. Computed (—) and measured (– –) H-plane beam patterns at 497 GHz, of a 4.0-mm-diameter silicon hemispherical lens with an extension length of 670 μm.

In Fig. 13, the results are shown for the lens without coating, and in Fig. 14 for the lens with a Stycast coating.

From these figures, it appears that the frequency dependence is more significant if no matching layer is present. For the noncoated lens, both the beamwidth and sidelobes change more as a function of frequency. Simulations for the same three frequencies do not show this trend. However, if the internally reflected field contributions are included into the model, the resulting beam patterns have a similar frequency-dependent behavior, as depicted as in Fig. 15.

Since the overall beam pattern is an effect of two (or more) contributions, i.e., the direct and internal reflection contributions, a change in frequency manifests itself as an interference pattern. Mainly the sidelobes are affected because the direct contribution is considerably stronger than the internal reflected field contribution. Even though the main beams are more or less

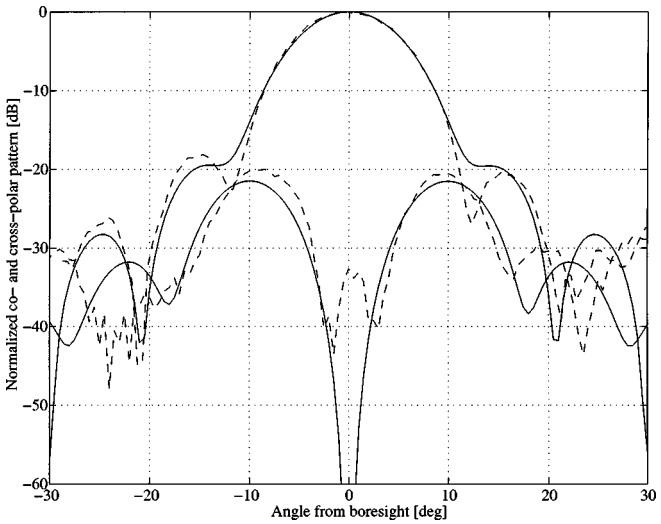

Fig. 9. Computed (—) and measured (– –) D-plane beam patterns at 497 GHz, of a 4.0-mm-diameter silicon hemispherical lens with an extension length of 670 μm.

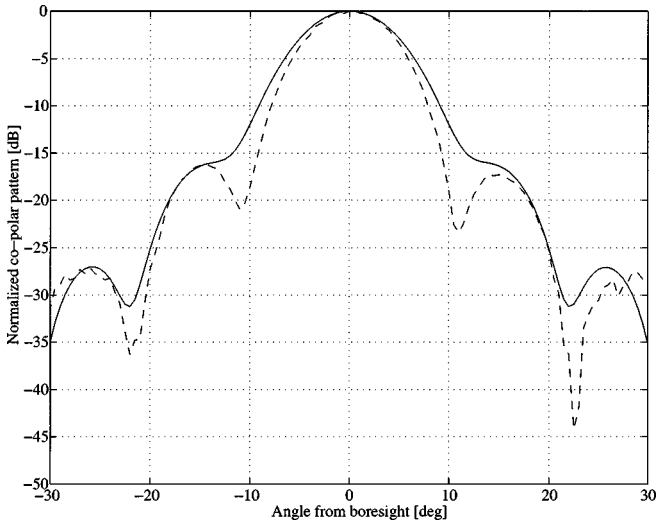

Fig. 10. Computed (—) and measured (– –) E-plane beam patterns at 497 GHz, of a 4.0-mm-diameter coated silicon hemispherical lens with an extension length of 670 μm.

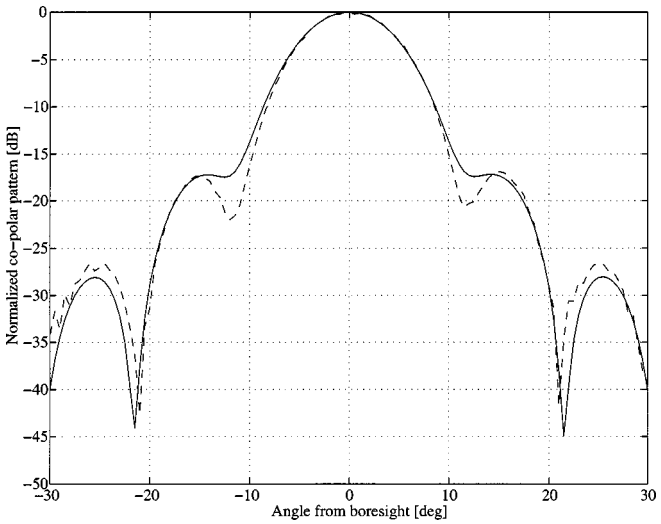

Fig. 11. Computed (—) and measured (– –) H-plane beam patterns at 497 GHz, of a 4.0-mm-diameter coated silicon hemispherical lens with an extension length of 670 μm.

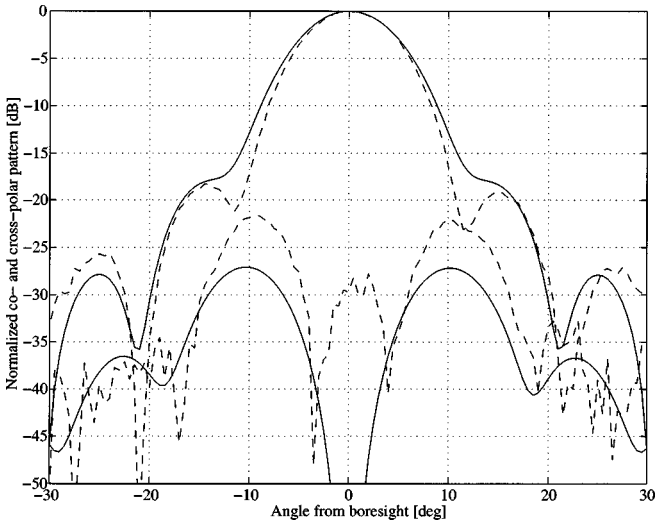

Fig. 12. Computed (—) and measured (– –) D-plane beam patterns at 497 GHz, of a 4.0-mm-diameter coated silicon hemispherical lens with an extension length of 670 μm.

unaffected, the beamwidth behavior is the same as can be observed from Fig. 13.

D. Results of the Beam and Gaussian Beam Efficiency

From the measured and predicted beams, it is possible to compute the beam and Gaussian beam efficiency. For the beam efficiency comparisons, the power in the main beam is computed to a level of -10 and -15 dB. In Table I, the resulting beam efficiencies are given. It should be noted that, for a fair comparison, only three φ-cuts (E-, D-, and H–planes) are taken from the measured and theoretical beam patterns for the computations of the efficiencies.

The agreement between the measured and predicted beam efficiencies is very good, except for the frequency of 486 GHz. This originates from the differences between both beam patterns (in E-, D-, and H-planes) at that frequency, but it is not clear what causes this discrepancy.

To compare the Gaussian beam efficiencies, the definition from [6] is used. However, it is clear from that reference that not only the far-field amplitude of the beam is needed, but also the far-field phase. The measurement setup described in Section III-A did not allow phase measurements. Therefore, to present the Gaussicity results, an uniform phase for both the computed and measured beams is assumed. This means that only the far-field amplitude is considered. In Table II, the results are shown for the Gaussicity and beam waist in the minimum waist plane.

The table clearly shows good agreement between the predicted and measured Gaussian beam efficiencies. In general, the beam waists are smaller (broader main beam) for the predicted beams than for the measured beams, which agrees with the observation from the beam patterns (Figs. 7–12). Further, it appears that the measured beams show the largest discrepancy

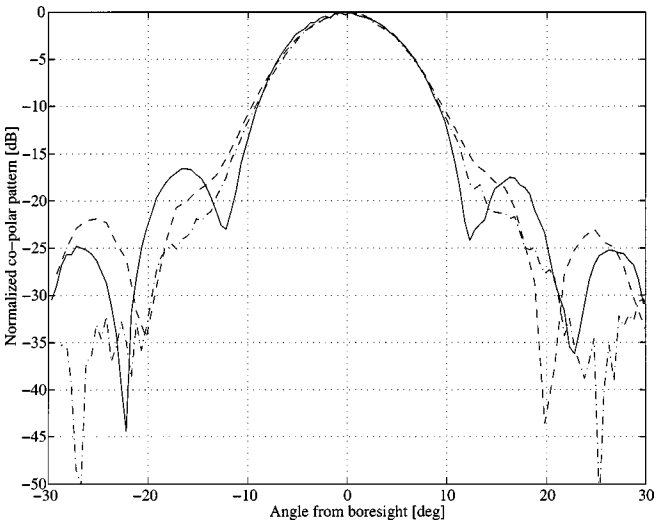

Fig. 13. Measured H-plane beam patterns [497 GHz (—), 486 GHz (– –), and 475 GHz (–.–)] for a 4.0-mm-diameter silicon hemispherical lens with an extension length of 670 μm.

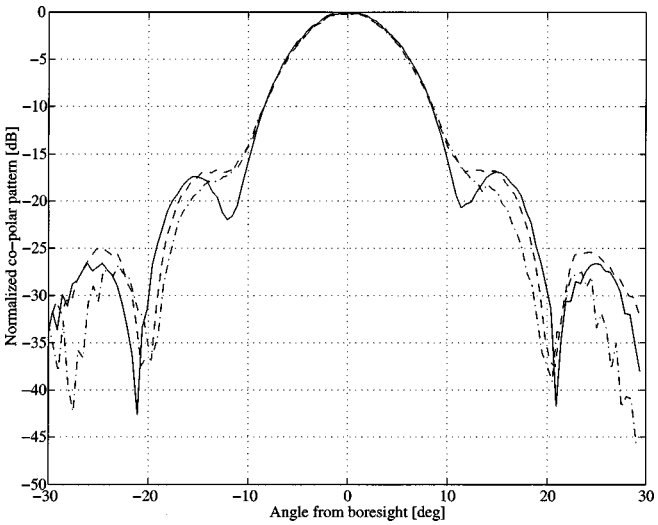

Fig. 14. Measured H-plane beam patterns [497 GHz (—), 486 GHz (– –), and 475 GHz (–.–)] for a 4.0-mm-diameter coated silicon hemispherical lens with an extension length of 670 μm.

with theory for a frequency of 486 GHz and this has also been observed from the beam efficiency comparisons.

V. Input Impedance Measurements

A. Description of Setup

The setup for the on-wafer S-parameter measurements of the double-slot feed is depicted in Fig. 16. In this figure, it can be seen that the CPW lines between the slots have been placed on the outside of the feed instead of on the inner side, as in the original double-slot design. The reason for this is that it is not possible to put the measurement probes on the wafer between the slots. It is, therefore, assumed that the S-parameters obtained in this way represent the double-slot feed with two CPW transformers at the inner side of the double slot. An extra length (1200 μm) of a transmission line is also added on both sides to prevent the on-wafer probes from influencing the measurements [10].

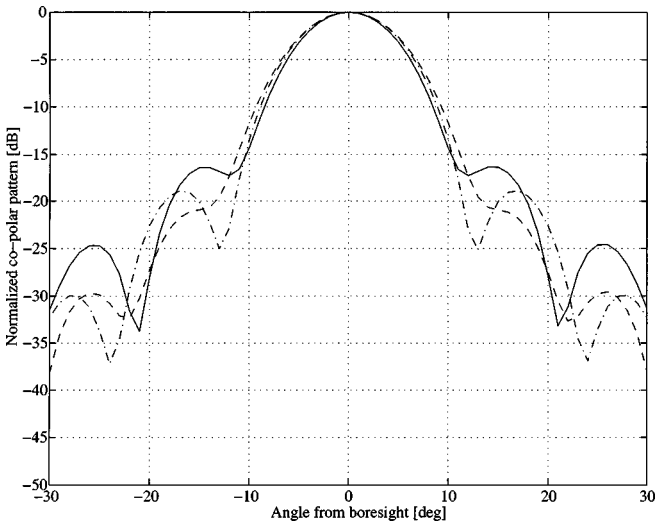

Fig. 15. Computed H-plane beam patterns [497 GHz (—), 486 GHz (– –), and 475 GHz (–.–)] for a 4.0-mm-diameter silicon hemispherical lens with an extension length of 670 μm. The first-order internal reflections are included.

TABLE I
Beam Efficiencies (Percentage) for the Measured and Predicted Beam Patterns

frequency [GHz]	matching [Yes/No]	measurements 10 dB	measurements 15 dB	predictions 10 dB	predictions 15 dB
497	No	83.8	88.4	83.9	88.9
486	No	74.9	83.1	83.1	88.5
475	No	82.9	89.3	83.1	88.6
497	Yes	83.0	87.4	82.4	88.6
486	Yes	78.4	83.2	81.7	88.5
475	Yes	82.6	88.8	81.7	88.1

TABLE II
Gaussicities (Percentage) and Beam Waists (in Millimeters) for the Measured and Predicted Beam Patterns

frequency [GHz]	matching [Yes/No]	measurements η_{gauss}	measurements w_0	predictions η_{gauss}	predictions w_0
497	No	90.8	1.30	94.0	1.25
486	No	85.3	1.19	93.7	1.26
475	No	93.2	1.29	93.5	1.27
497	Yes	91.3	1.35	94.9	1.16
486	Yes	89.2	1.28	94.7	1.17
475	Yes	94.3	1.34	94.5	1.18

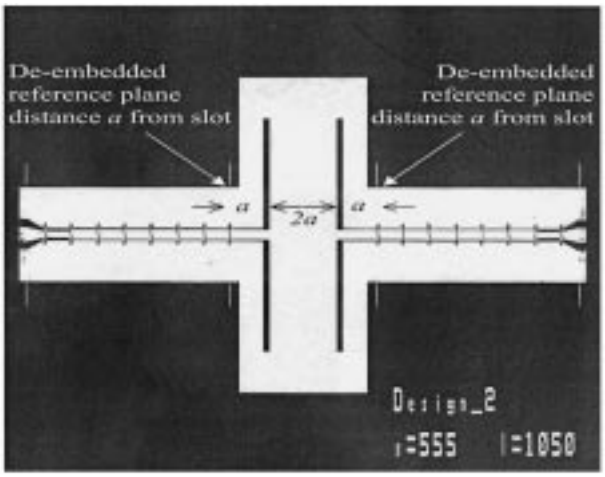

Fig. 16. Setup for the S-parameter measurements of the double-slot feed.

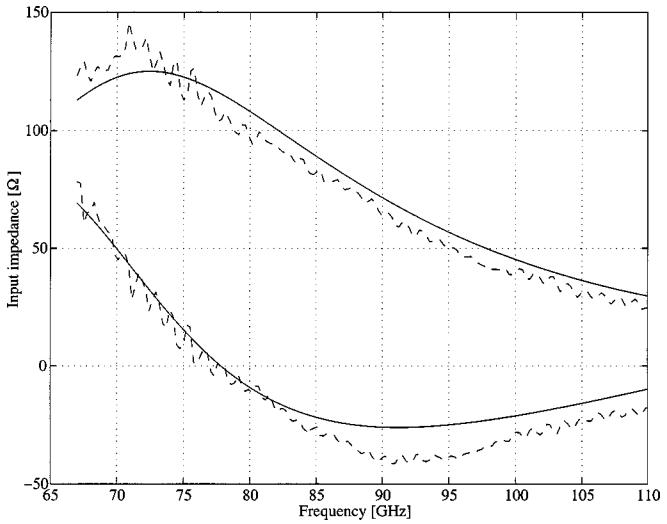

Fig. 17. Computed (—) and measured (– –) slot input impedance (in a double-slot configuration) for an off-axis feed displacement of 5.5 mm. The double slot is placed on a 20.0-mm-diameter silicon hemispherical lens with an extension of 3.35 mm.

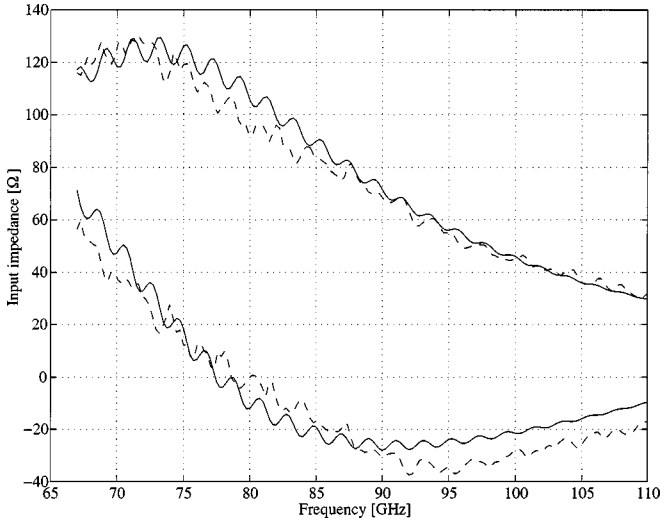

Fig. 18. Computed (—) and measured (– –) slot input impedance (in a double-slot configuration). The double slot is placed on a 20.0-mm-diameter silicon hemispherical lens with an extension of 3.35 mm.

B. Results for the Planar Feed

For the double-slot feed configuration with the extra CPW line, as depicted in Fig. 16, the impedance seen at the input port of one slot element is determined. Since the lens is present in the integrated lens antenna design used for the impedance measurements, its influence on this impedance can be predicted with the theoretical model described in [11]. Due to the lower frequency used for the input impedance measurements, the lens is a scaled version of the original lens and had a diameter of 20.0 mm instead of 4.0 mm.

The model of [11] was based on the assumption that all internally reflected waves would add up constructively only in the surrounding of the focal zone of the extended hemispherical lens. In view of this, it would not describe the input impedance alteration caused by the lens if the source is displaced with respect to the focus.

In order to verify the validity of this assumption, two different configurations of double slots on an extended hemispherical lens have been measured. First, the double-slot feed is placed at 5.5 mm off axis and, second, the double slot is placed in the focus itself. In the first case (Fig. 17), good agreement is found between the model and measured impedances, neglecting the lens effect. In the second case (Fig. 18), a good agreement is also found, but this time, by including the lens effect on the input impedance. The agreement between the predicted and observed oscillation is remarkable. This proves that the internally reflected waves are the main reason for the input impedance variations caused by the lens [6].

However, in the measured data of Fig. 17, small oscillations in the impedance can be observed as a function of frequency. These oscillations are certainly due to internal reflections, but the error that is introduced by neglecting them in the modeling is in the same order as the design of the double slot with the external CPW instead of the internal CPW.

VI. Conclusions

In this paper an integrated lens antenna was designed, which had a comparable performance as a Potter horn currently used in a limb-sounder receiver around 500 GHz. To verify the electromagnetic prediction models, measurements were conducted of the beam patterns around 500 GHz and scale-model measurements of the input impedance at 100 GHz. The co- and cross-polar beam-pattern measurements showed that, for a silicon lens with and without a Stycast ($\varepsilon_r = 2.9$) antireflection coating, the predicted patterns were comparable with the measured ones at three different frequencies, i.e., 475, 486, and 497 GHz. The effect of the internal reflections was noticeable when making a frequency sweep. Further, the predictions for the input impedance (from 67 to 110 GHz) agreed very well with the measured input impedances. Even the same oscillation with frequency, due to the lens effect, was observed for the input impedance of a single slot in a double-slot configuration.

Acknowledgment

The authors wish to thank N. Whyborn, Space Research Organization of the Netherlands, Groningen, The Netherlands, and S. Shitov, Space Research Organization of the Netherlands, Groningen, The Netherlands, for their contribution to the planar feed design and I. Thayne, University of Glasgow, Glasgow, Scotland, for performing the actual input impedance measurements.

References

[1] J. Zmuidzinas and H. G. LeDuc, "Quasi-optical slot antenna SIS mixers," *IEEE Trans. Microwave Theory Tech.*, vol. 40, pp. 1797–1804, Sept. 1992.

[2] S. S. Gearhart and G. M. Rebeiz, "A monolithic 250-GHz Schottky-diode receiver," *IEEE Trans. Microwave Theory Tech.*, vol. 42, pp. 2504–2511, Dec. 1994.

[3] D. F. Filipovic, S. S. Gearhart, and G. M. Rebeiz, "Double-slot antennas on extended hemispherical and elliptical silicon dielectric lenses," *IEEE Trans. Microwave Theory Tech.*, vol. 41, pp. 1738–1749, Oct. 1993.

[4] M. J. M. van der Vorst, "Integrated Lens Antennas for Submillimeter-wave Applications," Ph.D. dissertation, Elect. Eng. Dept., Eindhoven Univ. Technol., Eindhoven, The Netherlands, 1999.

[5] B. N. Ellison, M. L. Oldfield, D. N. Matheson, B. J. Maddison, C. M. Mann, and A. F. Smith, "Corrugated feedhorns at terahertz frequencies—Preliminary results," in *5th Int. Space Terahertz Technol. Symp.*, Ann Arbor, MI, 1994, pp. 851–860.
[6] M. J. M. van der Vorst, P. J. I. de Maagt, and M. H. A. J. Herben, "Effect of internal reflections on the radiation properties and input admittance of integrated lens antennas," *IEEE Trans. Microwave Theory Tech.*, vol. 47, pp. 1696–1704, Sept. 1999.
[7] R. Jorgensen, G. Padovan, P. de Maagt, D. Lamarre, and L. Costes, "Five-frequency millimeter wave antenna for a spaceborne limb sounding instrument," *IEEE Trans. Antennas Propagat.*, to be published.
[8] M. J. M. van der Vorst, P. J. I. de Maagt, and M. H. A. J. Herben, "On the design of integrated lens antennas," in *Proc. 20th ESTEC Millimeter Wave Antenna Technol. Antenna Meas. Workshop*, Noordwijk, The Netherlands, 1997, pp. 219–226.
[9] M. E. MacDonald and E. N. Grossman, "Niobium microbolometers for far-infrared detection," *IEEE Trans. Microwave Theory Tech.*, vol. 43, pp. 893–896, Apr. 1995.
[10] I. G. Thayne, D. L. Edgar, K. Elgaid, H. McLelland, S. Ferguson, A. Ross, J. M. Arnold, R. M. Heeres, N. Whyborn, W. Luinge, M. J. M. van der Vorst, A. Neto, and P. J. I. de Maagt, "On-wafer determination of the impedance of a planar 100 GHz double slot antenna," *Electron. Lett.*, vol. 35, pp. 1291–1292, 1999.
[11] A. Neto, S. Maci, and P. J. I. de Maagt, "Reflections inside an elliptical dielectric lens antenna," *Proc. Inst. Elect. Eng.*, pt. H, vol. 145, pp. 243–247, 1998.

Maarten J. M. van der Vorst (S'95–M'99) was born in Oudenbosch, The Netherlands, on November 12, 1970. He received the M.Sc. and the Ph.D. degrees from the Eindhoven University of Technology, Eindhoven, The Netherlands, in 1995 and 1999, respectively, both in electrical engineering.

He is currently with the European Space Research and Technology Centre (ESTEC), European Space Agency, Noordwijk, The Netherlands. His research interests include millimeter-wave and submillimeter-wave integrated antennas, design and analysis of lens and reflector antennas, and radar cross section modeling.

Peter J. I. de Maagt (S'88–M'88) was born in Pauluspolder, The Netherlands, in 1964. He received the M.Sc. and Ph.D. degrees from the Eindhoven University of Technology, Eindhoven, The Netherlands, in 1988 and 1992, respectively, both in electrical engineering.

He is currently with the European Space Research and Technology Centre (ESTEC), European Space Agency, Noordwijk, The Netherlands. His research interests are in the area of millimeter- and submillimeter-wave reflector and planar integrated antennas, quasi-optics, PBG antennas, and millimeter- and submillimeter-wave components.

Andrea Neto (S'98–M'99) was born in Naples, Italy, in 1968. He received the Laurea degree (*cum laude*) from the University of Florence, Florence, Italy, in 1994, and the Ph.D. degree from the University of Siena, Siena, Italy, in 1999, respectively, both in electronic engineering.

In 1995, he spent one year as a Young Graduate Trainee in the Antenna Section, Research and Technology Centre (ESTEC), European Space Agency (ESA), Noordwijk, The Netherlands. In October 1998, he rejoined the Antenna Section, Research and Technology Centre (ESTEC), European Space Agency (ESA), where his research is focused on high-frequency and numerical methods in electromagnetics, with emphasis on methods for the analysis of large arrays and integrated antennas.

Andrew L. Reynolds was born in Birmingham, U.K., in 1974. He received the European Master in electronics optoelectronics, M.Eng. (*cum laude*), and Ph.D. degrees from the University of Glasgow, Glasgow, Scotland, in 1996 and 2000, respectively.

In 1997, he spent one year as a Young Graduate Trainee in the Antenna Section, European Space Research and Technology Centre (ESTEC), European Space Agency (ESA), Noordwijk, The Netherlands. He is currently with the University of Glasgow. His research interests are focused on PBG materials to antenna and optoelectronic applications.

Rob M. Heeres was born in Den Helder, The Netherlands, in 1973. He received the M.Sc. degree in applied physics from the State University, Groningen, The Netherlands, in 1996.

In 1997 and 1998, he was a Physical Research Assistant at the Space Research Organization Netherlands Groningen, Groningen, The Netherlands. He is currently with Philips Discrete Semiconductors, Nijmegen, The Netherlands, where his research is focused on large-signal modeling of high-power RF transistors for the benefit of the design of power amplifiers.

Willem Luinge was born in Rolde, The Netherlands, in 1944. He received the M.Sc. degree in applied physics from the State University, Groningen, The Netherlands, in 1970.

He is currently with the Space Research Organization of the Netherlands (SRON), Groningen, The Netherlands. His interests are the development of instruments for application in and from space, most recently for the infrared and submillimeter spectral range.

Matti H. A. J. Herben (S'80–M'83–SM'88) was born in Klundert, The Netherlands, in 1953. He received the M.Sc. degree (*cum laude*) in electrical engineering and the Ph.D. degree in technical sciences from the Eindhoven University of Technology (EUT), Eindhoven, The Netherlands, in 1978 and 1984, respectively.

Since 1978, he has been with the Radiocommunications Group, EUT, where he is currently as an Associate Professor. His research interests and publications are in the areas of design and numerical analysis of reflector and lens antenna systems, radio interference reduction, electromagnetic-wave propagation on terrestrial and satellite links, remote sensing of the turbulent troposphere, and microwave radiometry.